Measurement of CO2 Diffusivity for Carbon Sequestration: A Microfluidic Approach for Reservoir-Specific Analysis

ARTICLE *in* ENVIRONMENTAL SCIENCE & TECHNOLOGY · OCTOBER 2012

Impact Factor: 5.33 · DOI: 10.1021/es303319q · Source: PubMed

4 AUTHORS, INCLUDING:

Hossein Fadaei
University of Toronto
27 PUBLICATIONS **138** CITATIONS
SEE PROFILE

Myeongsub Kim
Florida Atlantic University
17 PUBLICATIONS **57** CITATIONS
SEE PROFILE

David Sinton
University of Toronto
187 PUBLICATIONS **3,870** CITATIONS
SEE PROFILE

Environmental Science & Technology

Article

pubs.acs.org/est

Measurement of CO_2 Diffusivity for Carbon Sequestration: A Microfluidic Approach for Reservoir-Specific Analysis

Andrew Sell, Hossein Fadaei, Myeongsub Kim, and David Sinton*

Mechanical and Industrial Engineering and Centre for Sustainable Energy, University of Toronto, 5 King's College Road, Toronto, ON, Canada M5S 3G8

Supporting Information

ABSTRACT: Predicting carbon dioxide (CO_2) security and capacity in sequestration requires knowledge of CO_2 diffusion into reservoir fluids. In this paper we demonstrate a microfluidic based approach to measuring the mutual diffusion coefficient of carbon dioxide in water and brine. The approach enables formation of fresh CO_2–liquid interfaces; the resulting diffusion is quantified by imaging fluorescence quenching of a pH-dependent dye, and subsequent analyses. This method was applied to study the effects of site-specific variables—CO_2 pressure and salinity levels—on the diffusion coefficient. In contrast to established, macro-scale pressure–volume–temperature cell methods that require large sample volumes and testing periods of hours/days, this approach requires only microliters of sample, provides results within minutes, and isolates diffusive mass transport from convective effects. The measured diffusion coefficient of CO_2 in water was constant ($1.86\ [\pm 0.26] \times 10^{-9}$ m^2/s) over the range of pressures (5–50 bar) tested at 26 °C, in agreement with existing models. The effects of salinity were measured with solutions of 0–5 M NaCl, where the diffusion coefficient varied up to 3 times. These experimental data support existing theory and demonstrate the applicability of this method for reservoir-specific testing.

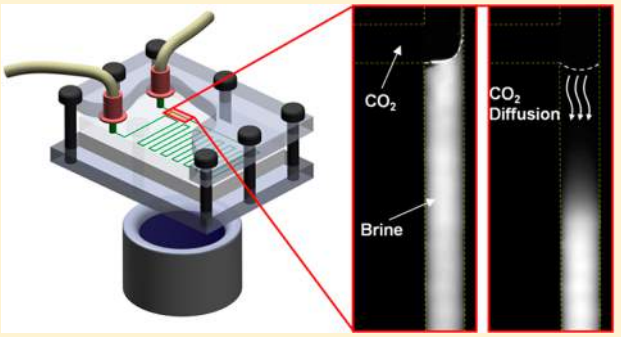

INTRODUCTION

Techniques aimed at mitigating atmospheric carbon dioxide (CO_2) are important for limiting anthropogenic CO_2 emissions linked to global warming. Storage of CO_2 in deep saline/brine aquifers is one mitigation technique currently being practiced.[1−3] In these storage projects, CO_2 is injected directly into a reservoir and trapped underground by three primary mechanisms:[4] (1) structural, (2) solubility, and (3) mineral trapping—where each consecutive mechanism is more secure (less chance for CO_2 leakage) than the previous.[5] Structural trapping is the least secure trapping mechanism and takes place when the buoyant migration of CO_2 is blocked by an impermeable layer of cap rock in a reservoir. Solubility trapping describes CO_2 dissolution into the resident fluid (carbonation); a mass transport limited process which is more secure than structural trapping since the CO_2 is no longer in its gaseous phase. Finally, the most secure trapping mechanism—mineral trapping—involves subsequent chemical reactions that occur to precipitate aqueous CO_2 into carbonates; if the aquifer/reservoir geochemistry is favorable.

Approximations of CO_2 storage security and capacity can be made by analyzing cap rock integrity, and determining the pore space available for structural trapping, respectively. For more accurate assessments of storage security/capacity, contributions from solubility and mineral trapping must also be considered. These trapping mechanisms are harder to quantify, however, because they are limited by mass transport—in particular diffusion—which takes hundreds of years to equilibrate. To lessen the uncertainty associated with these trapping mechanisms, above ground ex situ carbonation of reservoir fluids (followed by reinjection) has been proposed.[6] The feasibility of ex situ projects though is dependent on CO_2 dissolution rates (above ground resident time),[7−9] which are influenced by diffusion. Determining the mutual, Fick diffusion coefficient (D, equivalently diffusivity) between CO_2 and reservoir fluid is thus important to determine the long-term storage security/capacity of direct injection CO_2 storage sites and the viability of ex situ carbonation projects for carbon sequestration. This knowledge is essential for the assessment and acceptance of geological sequestration as a large scale CO_2 mitigation technique.[10]

Mutual diffusion coefficients of CO_2 in water are a well-documented function of relevant reservoir temperatures[11,12] and are even readily available for the pure water system at atmospheric pressures, however, there is considerable uncertainty regarding how the CO_2-water diffusion coefficient deviates under varying pressure and salinities—important conditions relevant to carbon sequestration. It is known by Henry's law that CO_2 concentration in solution is directly

Special Issue: Carbon Sequestration

Received: August 15, 2012
Revised: October 21, 2012
Accepted: October 23, 2012
Published: October 23, 2012

related to pressure. At low (≤1 bar) pressures it was shown that CO_2 concentrations are sufficiently dilute to not influence diffusivity,[13] as a result this assumption is commonly applied at higher CO_2 pressures as well.[14,15] Use of this assumption at higher pressures is considered valid since most diffusion models show diffusion coefficients depend significantly on solvent density and/or viscosity;[14,16,17] properties which, for water, change little with increased pressure. However, it has yet to be verified that diffusivity is constant with respect to concentration (pressure) under higher pressures. In terms of how salinity affects D—relatively little is established. When salinity levels in water increase, solution density increases, solubility of CO_2 is reduced,[18,19] and the dissociation constants change.[20] Hence, geochemistry of each underground aquifer is highly sensitive to salinity levels.[21] The change in CO_2 diffusivity with respect to salinity levels is predicted to occur since D is a function of water (solvent) association parameters as shown in a model by Garcia-Ratés et al.[15] One study[22] found that the *self-diffusion* of water changed in brine solutions—an indication that *mutual* diffusion coefficients should change as well. Furthermore, it was reported[23] that the apparent salt stress in plants lowers CO_2 diffusion. Although critical to CO_2 sequestration in saline aquifers, the influence of salinity on CO_2 diffusivity has yet to be quantified experimentally.

Traditional methods of determining CO_2 diffusion coefficients at high (reservoir like) pressures make use of pressure−temperature−volume (PVT) cells, primarily to monitor pressure decay. The pressure decay technique was pioneered by Riazi,[24] who developed it to measure gas diffusion into reservoir liquids. The major advantage of the pressure decay method for determining diffusivity is simplicity. However, it is prone to interpretation errors,[25] requires long (∼hours) run times, and does not capture the impact of concentration on the diffusion coefficient.[26] Also, because of the macro-scale nature of the conventional PVT technique, it can be difficult to isolate the diffusive process from density driven convective effects that develop in the test cell since CO_2-saturated water is more dense than water alone.[27] Several investigators[28−30] have studied the high pressure CO_2−water/brine system using PVT cells. While the effects of salinity were not investigated, they reported an increase in diffusivity as CO_2 pressure increased. Specifically, variances on the order of 2× were reported for pressure changes on the order of 10−50 bar. These results contradict most models of CO_2 diffusion into water which show little or no dependence on CO_2 concentration.[14,16,17] In another experiment,[31] the CO_2 diffusion coefficient in pure water was measured between only two pressures, 294 and 392 bar; no significant difference in diffusivity was observed, which is more agreeable with model predictions. Other investigators[32−35] have reported *apparent* diffusion coefficients; as a result of both diffusive and convective effects (owing to the large scale of traditional PVT testing vessels). Lindeberg and Wessel-Berg showed[36] the convective effect is highly dependent on reservoir porosity, to the point where low-porosity reservoirs would exhibit stable behavior and diffusion-dominated mass transfer. Even if convective flow were to develop in a reservoir, the onset is diffusion dependent,[37] signifying the importance of identifying the fundamental diffusion coefficient in the absence of convective effects present in large, conventional PVT measurement systems.

The objective of this work was to improve diffusion measurement methods for the CO_2−water system. Specifically, a novel microfluidic method was developed and applied to determine how the CO_2 diffusion coefficient changed as (a) pressure increased, and (b) salinity increased—two important parameters in the context of CO_2 sequestration. The approach measures diffusivity much faster than conventional PVT techniques, can operate at reservoir-relevant conditions, is amenable to multiplexing, and isolates diffusivity from convective effects. The implications for this type of diffusion measurement and the obtained data are discussed in the context of carbon sequestration.

EXPERIMENTAL METHODS

Materials, Fabrication, and Procedure. Microfluidic chips were made of two 25 × 25 × 3 mm pieces of poly(methyl methacrylate) (PMMA). The bottom piece had the microfluidic channel geometry ablated[38] onto it with a laser ablation system (Universal Laser) while the top piece was left blank. A solvent assist bonding method described elsewhere[39] was applied to seal the two chip pieces together. Upon completion, the chip was connected to a pressurized CO_2 tank and a purge line with nanoports (Upchurch Scientific) and clamped/sealed between two blank PMMA plates. Fluorescently tagged water/brine solutions were then injected into the chip, after initial solution pH had been measured.

Pure water was used to determine the effects of pressure on D (in the 5−50 bar range), while various molar concentrations (0−5) of reagent grade sodium chloride (NaCl) were made with deionized water to test the effects of salinity at constant pressure (5 bar). Testing solutions were tagged with sodium fluorescein tracer (Sigma Aldridch) at 200 μM. Fluorescein's fluorescence intensity depends on solution pH in the range of pH ∼3−7[40] where higher pH produces brighter signal. This pH range allows for visualization of the CO_2 front due to acidification caused by dissolution, and has been used previously to show gas transfer at windswept interfaces,[41] convective dissolution during flow,[42] and also diffusion.[31] During testing, pressure in the chip was monitored with a pressure transducer (Omegadyn, PX319) and 99.99% CO_2 (Linde) was supplied to the chip at desired testing pressures via a tank mounted regulator. All tests were run at 26 ± 1 °C.

Data: Acquisition and Handling. An inverted fluorescence microscope (DMI 6000B, Leica) fitted with a filter cube whose wavelength handling matched fluorescein's excitation and emission band was used to illuminate the sample. Images were captured using a CCD camera (Orca AG, Hamamatsu) and processed in an image processing program (ImageJ). To normalize captured fluorescence images, bright-field normalization was performed. Images then ran through a mean averaging filter using a rectangular kernel between 2 and 5 pixels. Finally, the images were imported into MATLAB (MathWorks Inc.) for analysis. A MatLab script was created to extract emission intensity data from the images (as a function of channel length) by averaging intensity values over the width of the channel. Once intensity profiles were obtained, pH profiles were found by exploiting the relationship between fluorescence intensity and solution pH. A calibration test achieved this, where normalized intensity values were plotted against known pH values with a nonlinear fit.

To calculate the CO_2 concentration causing the measured pH change, the following equilibrium/dissolution steps were used:

$$CO_{2(gas)} \leftrightarrow [CO_{2(aq)}] \quad (1)$$

dx.doi.org/10.1021/es303319q | Environ. Sci. Technol. 2013, 47, 71−78

$$[CO_{2(aq)}] + H_2O \leftrightarrow [H^+_{(aq)}] + [HCO^-_{3(aq)}] \quad (2)$$

$$[HCO^-_{3(aq)}] \leftrightarrow [H^+_{(aq)}] + [CO^{2-}_{3(aq)}] \quad (3)$$

During dissolution, the majority of dissolved CO_2 remains in its aqueous phase described by eq 1; governed by Henry's law. A small portion of aqueous CO_2 reacts with water to form bicarbonate ions ($HCO^-_{3(aq)}$) as shown in eq 2 (known as the first equivalent dissociation step), which increases $[H^+_{(aq)}]$—lowering pH and the fluorescence emission intensity. The equilibrium equation in eq 2 describes the equivalent dissociation when the carbonic acid $[CO_{2(aq)}] + H_2O \rightarrow [H_2CO_{3(aq)}]$ formation step is skipped since the presence of carbonic acid $[H_2CO_{3(aq)}]$ in solution is negligible due to its extremely fast dissociation.[43] The majority of the pH change observed in testing comes from the first equivalent dissociation (eq 2). The second dissociation step (eq 3) has a much smaller equilibrium constant, and could be neglected without incurring significant error, but is included in this formulation for the sake of completeness. The definitions for dissociation constants K_1 and K_2 then follow from above as follows:

$$K_1 = \frac{[H^+_{(aq)}][HCO^-_{3(aq)}]}{[CO_{2(aq)}]}$$

$$K_2 = \frac{[H^+_{(aq)}][CO^{2-}_{3(aq)}]}{[HCO^-_{3(aq)}]}$$

$$K_W = [H^+_{(aq)}][OH^-_{(aq)}] \quad (4)$$

Here the effect of water dissociation (K_w) is included. Though negligible for most pH ranges in consideration, water dissociation will contribute to $[H^+_{(aq)}]$ equilibrium in the event that starting pH values are high. Assuming charge neutrality of the solution:

$$0 = [H^+_{(aq)}] - [OH^-_{(aq)}] - [HCO^-_{3(aq)}] - 2[CO^{2-}_{3(aq)}] \quad (5)$$

and making appropriate substitutions from eq 4 into eq 5, $[CO_{2(aq)}]$ can be determined as a function of $[H^+_{(aq)}]$ with:

$$[CO_{2(aq)}] = \frac{[H^+_{(aq)}]^3 - K_W[H^+_{(aq)}]}{K_1([H^+_{(aq)}] + 2K_2)} \quad (6)$$

Equation 6 is applicable to study the diffusive process because the reactions used in its formulation are fast with respect to the diffusion time. Specifically, time scales on the order of 10 s are expected for local chemical equilibrium,[44] whereas the time scale for diffusion in our system (for $t \sim (l^2/D)$ with l = 1.5 mm, and $D = 10^{-9}$ m^2/s) is about 2000 s. The above representation for K_1 and K_2 assumes concentration and activity are equal; a valid assumption for very low salinity levels, but not accurate for tests run with increased salinity. Therefore, to take into account the activity change as salinity increases, an ion activity model provided by Millero et al.[45] was used to calculate values for K_1 and K_2 as a function of temperature and salinity. Equation 6 is an established relation for changes in solution pH due to dissolved CO_2, and has been used in a variety of fluorometric CO_2 sensors.[46−49] By utilizing a known calibration solution to obtain pH values from captured intensity values, CO_2 concentration can be calculated with eq 6 at any location and time within the microchannel.

Determining the Diffusion Coefficient—Analytical Fitting to Experimental Data. To acquire a diffusivity value from tests, the obtained CO_2 concentration data must be fit to an analytical diffusion model. The analytical model was based on a semi-infinite one-dimensional diffusive process—a valid assumption since the channel length is orders of magnitude higher than the diffusive length. Initially, CO_2 concentration in solution is assumed everywhere 0 and the concentration at infinity (c_∞) for all times is set to 0 (due to the long channel geometry). As soon as $t = 0^+$ CO_2 concentration at the interface instantly changes from 0 to c_0, the saturation concentration, for the corresponding test pressure. The analytical model also assumes that the diffusion coefficient, D, does not vary significantly in response to CO_2 concentration (dilute assumption). In the experiments, dependence on CO_2 concentration would be apparent due to a lack of fit with this model. With these assumptions and initial/boundary conditions, the solution to Fick's second law, given by Crank,[50] is applied to model CO_2 concentration, c, within the water in the microchannel by:

$$c = c_0 erfc(\zeta) \quad (7)$$

where $erfc(\zeta)$ is the complementary error function defined by $1 - erf(\zeta)$ and $\zeta = (z/(4Dt)^{1/2})$. Here z is the coordinate in the direction of the diffusive process, and D and t are the Fick diffusion coefficient and time, respectively. Utilizing a nonlinear least-squares fitting algorithm, the CO_2 concentration data is fit with eq 7 for every time-step captured, with D being the fitting parameter. The fugacity of CO_2 can be assumed equivalent to total pressure at conditions below the critical point and can be used as a simplifying assumption to determine the saturation concentration, c_0. However, to ensure higher accuracy and compatibility with increased test pressures, the saturation concentration, c_0, in eq 7 was calculated as a function of temperature, pressure (fugacity), and potential salinity with the model developed by Duan et al.[51]

RESULTS AND DISCUSSION

Figure 1a shows the microfluidic system developed here, consisting of a patterned microchip clamped between polymer plates and connected to high pressure CO_2. The channel design on the microchip allows the user to dynamically control the two-phase fluid interface by throttling a plug valve downstream of the chip. The chip design includes a long fluidic resistor that serves as a fluid reservoir to continually supply fresh, non-CO_2-saturated water to the interface. This design ensures a valid initial condition (i.e., fresh CO_2−liquid interface) is obtained when the plug valve is closed. The back pressure provided by proximity of the resistor inlet/outlet immobilizes the interface during diffusion testing. A detailed diagram of this flow operation is shown in Figure 1b.

There are three reasons the diffusion process is isolated from convective effects in this microfluidic setup: (1) Gravity acts perpendicular to the diffusion direction (and the density gradient), thereby eliminating any density-driven convective effects throughout the length of the microchannel. (2) Because of the small channel dimensions of the microchip (depth ∼50 μm, width ∼100 μm), the Rayleigh number (Ra) for the system falls below the critical Rayleigh number (Ra = 67.94), ensuring free convection will not occur.[52] (3) The capillary pressure that confines the brine test fluid within the channel is high, which guarantees any interfacial body forces induced by the density changes will be negligible by comparison. Furthermore, no

dx.doi.org/10.1021/es303319q | Environ. Sci. Technol. 2013, 47, 71−78

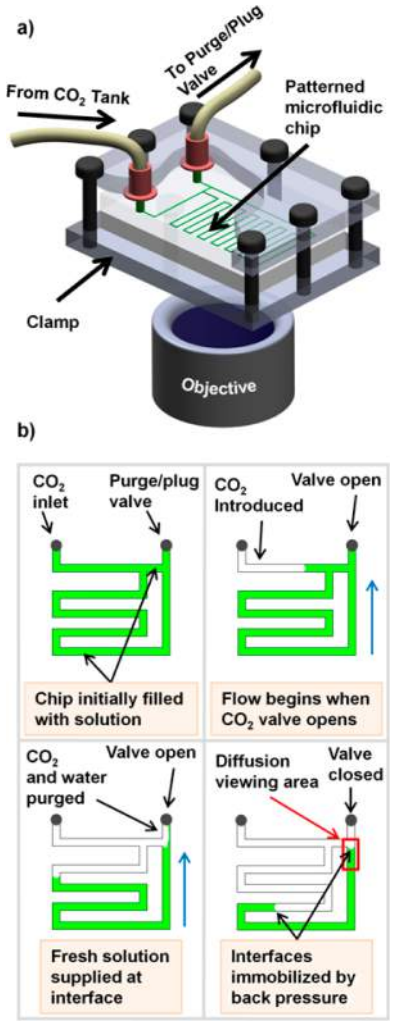

Figure 1. Microfluidic system used to determine CO_2 diffusion coefficients in water. (a) Schematic of the experimental setup. The microfluidic chip is contained in a clamping device which seals the inlet and outlet ports, allowing high-pressure CO_2 to be interfaced with the chip. The entire setup is placed on an inverted fluorescence microscope with a wide field-of-view objective for imaging. (b) Schematic of the CO_2 diffusivity test initialization procedure. Initially the chip is flooded with green fluorescent solution (top left). The purge valve is opened and pure CO_2 is introduced into the chip (top right). As long as the purge valve is open, CO_2 will flow through the fluidic resistor, pushing both CO_2 and the liquid out the purge valve (bottom left). As soon as the purge valve is closed, the interfaces are immobilized by the confining pressure (bottom right). Diffusion is then viewed at the highlighted location under the fluorescence microscope. The procedure can be repeated several times, provided there is sufficient solution in the reservoir.

convective effects were visible during experimentation. Such effects would have been apparent due to the ability to detect trace amounts of CO_2 in the liquid phase with the fluorescent tracer, and/or a deviation from classic diffusive behavior; however these effects were not observed. The design of the microchip is fundamentally different from previous microfluidic approaches to diffusion measurement using the T-Sensor,[53] and enables assessment of diffusion coefficients in stagnant fluid, without complications from flow or cross-stream velocity gradients. The method is also straightforward to run as it requires only a single high-pressure source which, through the chip design, provides controlled flow of *both* liquid and gas constituents as required.

Figure 2 shows an image time sequence as CO_2 diffused into water, acidified it, and quenched the fluorescence. The pH

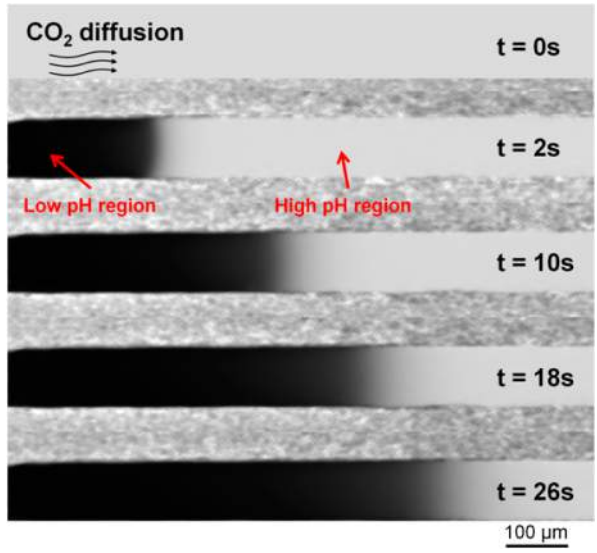

Figure 2. Time-lapse images showing fluorescent quenching as CO_2 diffuses into water and acidifies the solution. The water initially fluoresces uniformly (t = 0 s), but when CO_2 comes into contact with the solution on the left-hand side (the interface is located off the left, ~20 μm, of the figure), diffusion proceeds into the water, lowering the solution pH and quenching the fluorescent signal (t = 2–26 s). P = 5 bar. See Supporting Information for a video of the process.

change took place as CO_2 diffused into solution, in the channel. As can be seen in the figure, the process is highly one-dimensional, as required for the theoretical treatment (eq 7). Figure 3 shows the averaged, cross-channel emission intensities, as well as subsequent calibration/calculation plots for four time-steps obtained during a single test. Data were obtained at a distance (~150 μm) from the interface to avoid any lensing effects caused by the curvature of the CO_2–water interface.[54] The emission intensities shown in Figure 3 were first mapped to pH data through calibration, then the corresponding CO_2 concentration profile was calculated with eq 6. The CO_2 concentrations are given on a molar basis (mol/L) instead of molal (mol/kg), this was done to simplify calculations during the fitting process. Because of the relative incompressibility of water,[55] the error associated with utilizing molarity instead of molality (and therefore neglecting the increase in density—volume change—as pressure increases) is only 0.28% for the max testing pressure used in this paper (50 bar). At 500 bar the error is 4%, hence if the setup is modified to handle extreme conditions, any testing done in excess of 500 bar should consider the density change by making use of molality to help mitigate errors. Each CO_2 concentration curve in a given test can then be fit to the analytical solution of the diffusion equation (eq 7).

Figure 4 shows measured CO_2 concentration profiles and the analytical functions (eq 7) corresponding to the best-fit D values as indicated. Fluorescent signal-to-noise ratio is lower in low pH (~3.3) regions near the interface, resulting in a deviation from the analytical function as shown. The deviation is not substantial, but to account for the noise error, a weighting function was applied based on the standard deviation from the

dx.doi.org/10.1021/es303319q | *Environ. Sci. Technol.* 2013, 47, 71–78

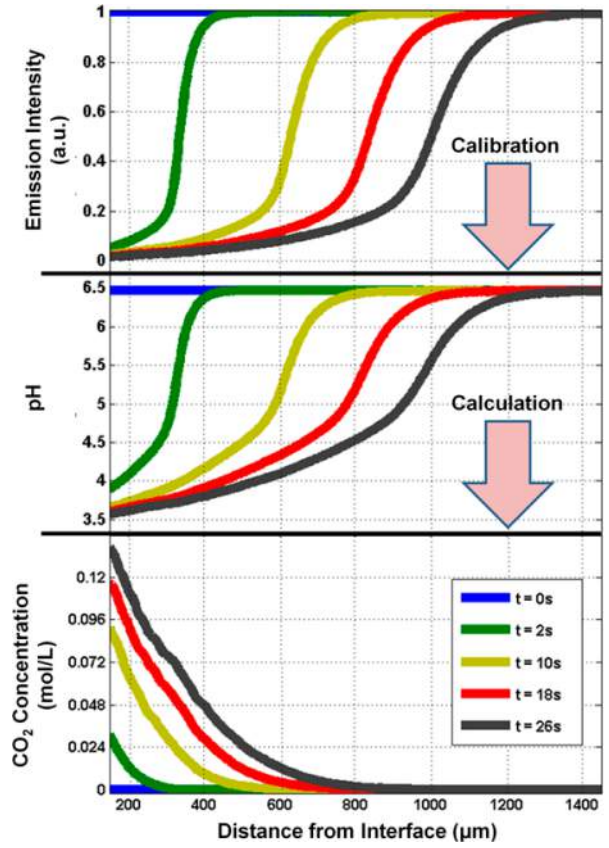

Figure 3. Measured cross-channel profile plots for intensity, pH, and CO_2 concentration along the microchannel (averaged in the cross-section). The profiles were obtained first by averaging emission intensity observed across the channel width (top plot). Through calibration, pH profiles (center plot) were mapped to respective intensity values. Finally, a calculation step (eq 6) yielded the CO_2 concentration for each time period (bottom plot). P = 5 bar. Lines appear thick due to high density of data points.

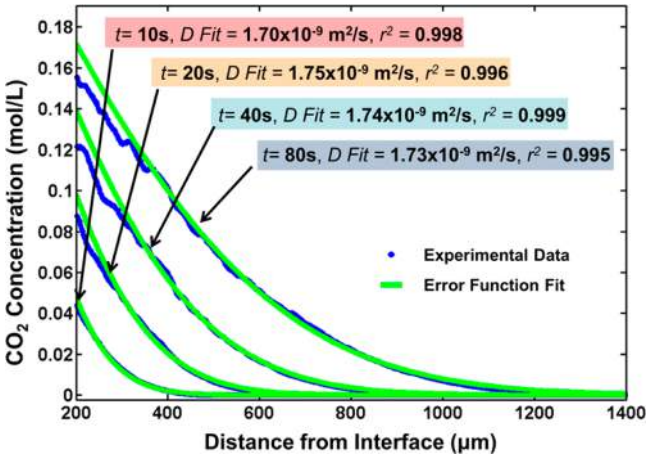

Figure 4. Comparison of measured CO_2 concentration curves with the analytical model for selected time-steps. Here the diffusion coefficient is determined based on the best analytical fit (eq 7) to measured CO_2 concentration curves. Average r^2 values for the fitting parameter ranged between 0.94 and 0.99 for all tests/times run, as shown inset. Note the color scheme for each time-step, these colors correspond to the same data/times shown in Figure 5. P = 5 bar.

mean intensity values measured. As shown, measured profiles match the analytical model quite well over the channel length, as indicated by the fit coefficients shown inset.

An example of all diffusion coefficients obtained for a single experimental run is shown in Figure 5. Each data point is 2 s apart (corresponding to the imaging frame rate) and as can be seen, D values at initial times are lower, and exhibit relatively large error. This increased error is partly due to inaccuracies in initial timing (±0.2 s, the time when the purge valve is closed and when diffusion begins) and interface development/stabilization effects. After ~10 s these errors reduce and all the data points fall into good agreement with an average individual error of 5−7%. The predicted error is a function of various measurements used in the experimental method and includes the following: uncertainty in initial pH measurements, saturation concentration, and pressure/temperature readings and fluctuations. The overall D value is obtained by averaging all diffusion coefficients obtained past this initial development period, in this case (where P = 5 bar), $D = 1.74\ [\pm 0.15] \times 10^{-9}$ m^2/s.

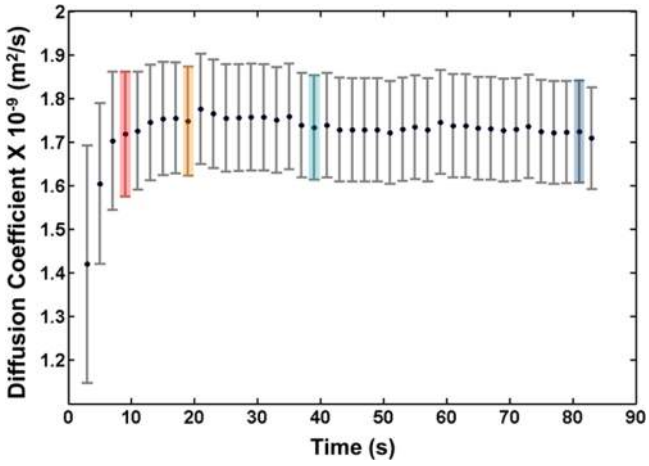

Figure 5. Diffusion coefficients obtained at 5 bar. A diffusion coefficient is determined for each frame captured during experimentation. Here, each data point (frame) is 2 s apart. The error bars represent the uncertainty involved in measurements made during testing (e.g., initial pH, temperature), and how they impact the resulting D. An overall D value for this pressure is obtained by averaging these D values, giving a $D = 1.74 \times 10^{-9}$ m^2/s. Selected data points are shown with the same color scheme given in Figure 4 for cross reference.

To measure the impact of pressure on diffusivity, several tests were run at incremental pressures; results are plotted in Figure 6. The individual error for each pressure tested includes the estimated base measurement errors shown in Figure 5, and also includes errors from averaging D values for a specific test. Individual test errors were primarily from slight interfacial movements due to pressure fluctuations from the CO_2 tank and/or residual film flow at early time-steps. As a result, a maximum uncertainty of 6−14% was obtained. When compared to the well-known Wilke-Chang correlation[16] for dilute diffusion as well as a recent model developed by Mutoru et al.[14] we see good agreement, with no consistent change in D as pressure increases. The change in the diffusion coefficient with respect to pressure is negligible, and therefore can be assumed constant for the range of pressures tested here. Taking the mean value gives a $D = 1.86\ [\pm 0.26] \times 10^{-9}$ m^2/s.

dx.doi.org/10.1021/es303319q | Environ. Sci. Technol. 2013, 47, 71−78

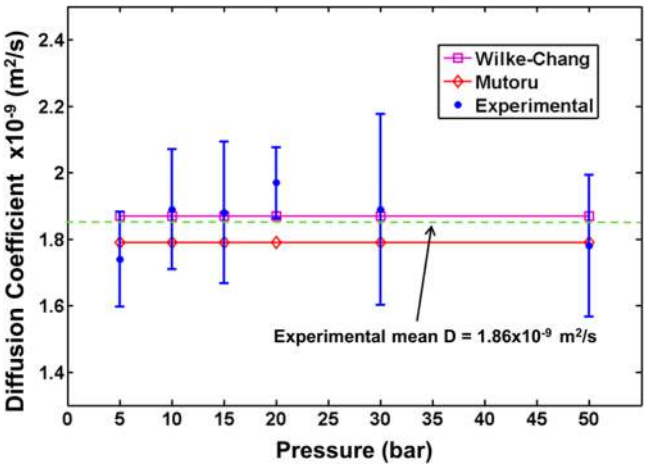

Figure 6. CO_2–water diffusion coefficient measured as a function of pressure, with values at 5, 10, 15, 20, 30, and 50 bar. Error bars indicate the confidence in each measurement and reflect uncertainty in temperature, pressure, and pH measurements, as well as taking into account any slight interfacial movements occurring in a given test. There is no significant trend observed for D as pressure increases. A mean of the obtained values gives $D = 1.86\ [\pm 0.26] \times 10^{-9}$ m^2/s, which is agreeable with models provided by Wilke-Chang[16] and Mutoru et al.[14].

Figure 7 shows measured CO_2–brine diffusivity values as a function of salinity. Results show salinity has a significant influence on obtained D values, where D decreases as salinity levels increase. The diffusion coefficient drops by a factor of ~3 between pure water and 5 M NaCl. These experimental results support most models for diffusivity that include a dependence on solvent association parameters. The drop in the diffusion coefficient is also in line with predictions given by the molecular simulation results provided by Garcia-Rates et al.[15] Any additional effects of other dissolved solids/salts, as present in a given reservoir, could readily be analyzed by employing the technique developed here.

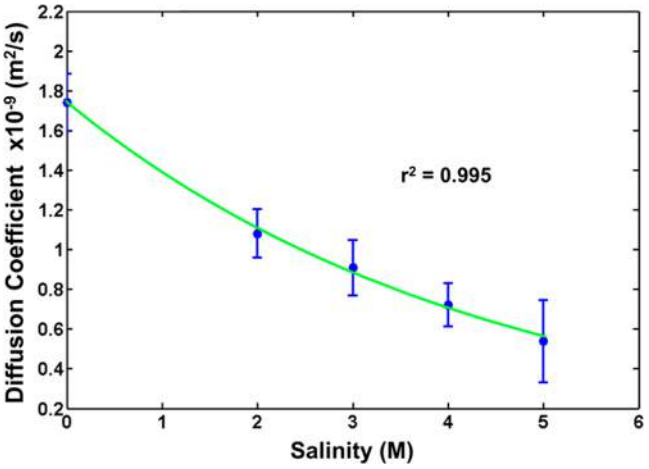

Figure 7. CO_2–brine diffusion coefficients as a function of salinity. Data show a decrease in the diffusion coefficient as salinity increases. An exponential fit is shown which can relate the effects of salinity on the diffusion coefficient $[D = (1.75 \times 10^{-09})(e^{-0.229 \times \text{Salinity}})]$. The correlation is intended as an estimation tool, and is only applicable for the temperature used in this analysis. $P = 5$ bar.

Regarding the temperature and pressure range employed to validate the method, two aspects are noteworthy: (a) the working temperature here is below those expected in geologic sequestration formations, and (b) the pressure range up to 50 bar is not as high as typical CO_2 sequestration operations. Though these conditions may be applicable to ex situ processes, this measurement method is well suited to study a full range of temperatures using established microfluidic temperature control methods.[56,57] The method is also applicable to much higher pressures, as on-chip processes have been demonstrated using similar glass/silicon chips at pressures up to 25 MPa.[58,59] Utilizing proven temperature controlled practices with a proven high pressure design would allow these tests to be run under a wide range of relevant conditions.

Implications. Microfluidics and pH-induced fluorescence quenching enable the rapid determination of CO_2 diffusivity in reservoir fluids. The most significant implication of this work is in the demonstration of efficacy and speed at which diffusivity tests can be run, enabling rapid reservoir-specific tests. Diffusivity measurements were achieved in less than 90 s, as compared to hours or days with conventional methods. Under the conditions studied, it was found that pressure had no significant effect on diffusion rates (no dependence on CO_2 concentration within the solution). This finding supports an assumption applied by many sequestration models—that time scales for dissolution are largely independent of reservoir depth (or ex situ carbonation pressures). The provided results also elucidate the influence salinity has on the diffusive process. Measurements verify that a reservoir with high salinity levels will experience slower diffusion rates—up to 3 times slower. While the individual example tests provide insight, the results obtained here demonstrate a rapid and accurate method with potential to inform carbon management through rapid reservoir-specific diffusivity analysis.

■ ASSOCIATED CONTENT

Supporting Information

A video showing the microfluidic diffusion process taking place as CO_2 quenches the fluorescent signal. This information is available free of charge via the Internet at http://pubs.acs.org.

■ AUTHOR INFORMATION

Corresponding Author

*E-mail: sinton@mie.utoronto.ca; phone: (416) 978-1623; fax: (416) 978-7753.

Notes

The authors declare no competing financial interest.

■ ACKNOWLEDGMENTS

We gratefully acknowledge funding from Carbon Management Canada, Theme B: Emerging Technologies, Project B-04, and ongoing funding from the Natural Science and Engineering Research Council of Canada (NSERC). We also gratefully acknowledge infrastructure funding from the Canada Foundation for Innovation (CFI), and helpful discussions with Professor John M. Shaw.

■ REFERENCES

(1) Iding, M.; Ringrose, P. Evaluating the impact of fractures on the long-term performance of the In Salah CO_2 storage site. *Energy Procedia* **2009**, *1*, 2021–2028.

(2) Kongsjorden, H.; Kårstad, O.; Torp, T. A. Saline aquifer storage of carbon dioxide in the Sleipner project. *Waste Manage.* **1998**, *17*, 303−308.
(3) Chadwick, A.; Arts, R.; Bernstone, C.; May, F.; Thibeau, S.; Zweigel, P. Best Practice for the Storage of CO_2 in Saline Aquifers-Observations and Guidelines from the SACS and CO2STORE projects. *Br. Geol. Surv.* **2008**, *14*, 267.
(4) Bachu, S. CO_2 storage in geological media: Role, means, status and barriers to deployment. *Prog. Energy Combust. Sci.* **2008**, *34*, 254−273.
(5) Dilmore, R. M.; Allen, D. E.; Jones, J. R. M.; Hedges, S. W.; Soong, Y. Sequestration of Dissolved CO_2 in the Oriskany Formation. *Environ. Sci. Technol.* **2008**, *42*, 2760−2766.
(6) Leonenko, Y.; Keith, D. W. Reservoir Engineering To Accelerate the Dissolution of CO_2 Stored in Aquifers. *Environ. Sci. Technol.* **2008**, *42*, 2742−2747.
(7) Gerdemann, S. J.; O'Connor, W. K.; Dahlin, D. C.; Penner, L. R.; Rush, H. Ex Situ Aqueous Mineral Carbonation. *Environ. Sci. Technol.* **2007**, *41*, 2587−2593.
(8) Zendehboudi, S.; Leonenko, Y.; Shafiei, A.; Soltani, M.; Chatzis, I. Modeling of CO_2 droplets shrinkage in ex situ dissolution approach with application to geological sequestration: Analytical solutions and feasibility study. *Chem. Eng. J.* **2012**, *197*, 448−458.
(9) Zendehboudi, S.; Khan, A.; Carlisle, S.; Leonenko, Y. Ex Situ Dissolution of CO_2: A New Engineering Methodology Based on Mass-Transfer Perspective for Enhancement of CO_2 Sequestration. *Energy Fuels* **2011**, *25*, 3323−3333.
(10) Wallquist, L.; Visschers, V. H. M.; Siegrist, M. Impact of knowledge and misconceptions on benefit and risk perception of CCS. *Environ. Sci. Technol.* **2010**, *44*, 6557−62.
(11) Thomas, W. J.; Adams, M. J. Measurement of the diffusion coefficients of carbon dioxide and nitrous oxide in water and aqueous solutions of glycerol. *Trans. Faraday Soc.* **1965**, *61*, 668.
(12) Tamimi, A.; Rinker, E. B.; Sandall, O. C. Diffusion Coefficients for Hydrogen Sulfide, Carbon Dioxide, and Nitrous Oxide in Water over the Temperature Range 293−368 K. *J. Chem. Eng. Data* **1994**, *39*, 330−332.
(13) Tang, Y.; Himmelblau, D. Effect of solute concentration on the diffusivity of carbon dioxide in water. *Chem. Eng. Sci.* **1965**, *20*, 7−14.
(14) Mutoru, J. W.; Leahy-Dios, A.; Firoozabadi, A. Modeling infinite dilution and Fickian diffusion coefficients of carbon dioxide in water. *AIChE J.* **2011**, *57*, 1617−1627.
(15) Garcia-Ratés, M.; de Hemptinne, J. C.; Avalos, J. B.; Nieto Draghi, C. Molecular Modeling of Diffusion Coefficient and Ionic Conductivity of CO_2 in Aqueous Ionic Solutions. *J. Phys. Chem. B* **2012**, *116* (9), 2787−2800.
(16) Wilke, C. R.; Chang, P. Correlation of diffusion coefficients in dilute solutions. *AIChE J.* **1955**, *1*, 264−270.
(17) Brokaw, R. S. Predicting Transport Properties of Dilute Gases. *Ind. Eng. Chem. Process Des. Dev.* **1969**, *8*, 240−253.
(18) Takenouchi, S.; Kennedy, G. C. The solubility of carbon dioxide in nacl solutions at high temperatures and pressures. *Am. J. Sci.* **1965**, *263*, 445−454.
(19) Chang, Y.-B.; Coats, B.; Nolen, J. A Compositional Model for CO_2 Floods Including CO_2 Solubility in Water. *SPE Reservoir Eval. Eng.* **1998**, *1*, 155−160.
(20) Li, D.; Duan, Z. The speciation equilibrium coupling with phase equilibrium in the H_2O−CO_2−NaCl system from 0 to 250 °C, from 0 to 1000 bar, and from 0 to 5 molality of NaCl. *Chem. Geol.* **2007**, *244*, 730−751.
(21) Shao, H.; Ray, J. R.; Jun, Y.-S. Effects of Salinity and the Extent of Water on Supercritical CO(2)-Induced Phlogopite Dissolution and Secondary Mineral Formation. *Environ. Sci. Technol.* **2011**, *45*, 1737−1743.
(22) Yechieli, Y.; Ronen, D. Self-diffusion of water in a natural hypersaline solution (Dead Sea brine). *Geophys. Res. Lett.* **1996**, *23*, 845−848.
(23) Delfine, S.; Alvino, A.; Zacchini, M.; Loreto, F. Consequences of salt stress on conductance to CO_2 diffusion, Rubisco characteristics and anatomy of spinach leaves. *Aust. J. Plant Physiol.* **1998**, *25*, 395−402.
(24) Riazi, M. R. A new method for experimental measurement of diffusion coefficients in reservoir fluids. *J. Pet. Sci. Eng.* **1996**, *14*, 235−250.
(25) Tharanivasan, A. K.; Yang, C.; Gu, Y. Comparison of three different interface mass transfer models used in the experimental measurement of solvent diffusivity in heavy oil. *J. Pet. Sci. Eng.* **2004**, *44*, 269−282.
(26) Zhang, X.; Shaw, J. M. Liquid-phase Mutual Diffusion Coefficients for Heavy Oil + Light Hydrocarbon Mixtures. *Pet. Sci. Technol.* **2007**, *25*, 773−790.
(27) Teng, H.; Yamasaki, A. Solubility of Liquid CO_2 in Synthetic Sea Water at Temperatures from 278 to 293 K and Pressures from 6.44 to 29.49 MPa, and Densities of the Corresponding Aqueous Solutions. *J. Chem. Eng. Data* **1998**, *43*, 2−5.
(28) Renner, T. Measurement and correlation of diffusion coefficients for CO_2 and rich-gas applications. *SPE Reservoir Eng.* **1988**, *3* (2), 517−523.
(29) Wang, L.; Lang, Z. Measurement and correlation of the diffusion coefficients of carbon dioxide in liquid hydrocarbons under elevated pressures. *Fluid Phase Equilib.* **1996**, *117*, 364−372.
(30) Bahar, M.; Liu, K. Measurement of the Diffusion Coefficient of CO_2 in Formation Water under Reservoir Conditions: Implications for CO_2 Storage. *SPE Asia Pacific Oil and Gas Conference and Exhibition* **2008**, 1−8.
(31) Hirai, S.; Okazaki, K.; Yazawa, H.; Ito, H.; Tabe, Y.; Hijikata, K. Measurement of CO_2 diffusion coefficient and application of LIF in pressurized water. *Energy* **1997**, *22*, 363−367.
(32) Yang, C.; Gu, Y. Accelerated Mass Transfer of CO_2 in Reservoir Brine Due to Density-Driven Natural Convection at High Pressures and Elevated Temperatures. *Ind. Eng. Chem. Res.* **2006**, *45*, 2430−2436.
(33) Farajzadeh, R.; Zitha, P. L. J.; Bruining, J. Enhanced Mass Transfer of CO_2 into Water: Experiment and Modeling. *Ind. Eng. Chem. Res.* **2009**, *48*, 6423−6431.
(34) Neufeld, J.; Hesse, M. Convective dissolution of carbon dioxide in saline aquifers. *Geophys. Res. Lett.* **2010**, *37*, 1−5.
(35) Emami Meybodi, H. Comments on the Paper "Quantification of Density-Driven Natural Convection for Dissolution Mechanism in CO2 Sequestration" by R. Nazari Moghaddam et al. (2011). *Transp. Porous Media* **2012**, *93*, 171−174.
(36) Lindeberg, E.; Wessel-Berg, D. Vertical convection in an aquifer column under a gas cap of CO_2. *Energy Convers. Manage.* **1997**, *38*, S229−S234.
(37) Xu, X.; Chen, S.; Zhang, D. Convective stability analysis of the long-term storage of carbon dioxide in deep saline aquifers. *Adv. Water Res.* **2006**, *29*, 397−407.
(38) Klank, H.; Kutter, J. P.; Geschke, O. CO(2)-laser micromachining and back-end processing for rapid production of PMMA-based microfluidic systems. *Lab Chip* **2002**, *2*, 242−6.
(39) Ogilvie, I. R. G.; Sieben, V. J.; Floquet, C. F. A.; Zmijan, R.; Mowlem, M. C.; Morgan, H. Reduction of surface roughness for optical quality microfluidic devices in PMMA and COC. *J. Micromech. Microeng.* **2010**, *20*, 065016.
(40) Martin, M. M.; Lindqvist, L. The pH dependence of fluorescein fluorescence. *J. Lumin.* **1975**, *10*, 381−390.
(41) Takehara, K.; Etoh, G. T. *A Direct Visualization Method of CO_2 Gas Transfer at Water Surface Driven by Wind Waves*; Donelan, M. A.; Drennan, W. M.; Saltzman, E. S.; Wanninkhof, R., Eds.; American Geophysical Union: Washington, DC, 2002; Vol. *127*, pp 89−95.
(42) Senga, Y.; Tsutsui, I.; Mishima, K.; Kakinuma, Y.; Sato, Y. CO_2 Dissolution Process At Gas-Liquid Interface In Two Phase Microchannel Flow. In *Proceedings of PowerMEMS 2008+ microEMS2008*; 2008.
(43) Espinoza, D. N.; Santamarina, J. C. Water-CO_2 -mineral systems: Interfacial tension, contact angle, and diffusion—Implications to CO_2 geological storage. *Water Resour. Res.* **2010**, *46*, 1−10.

(44) Zeebe, R. E.; Wolf-Gladrow, D. A.; Jansen, H. On the time required to establish chemical and isotopic equilibrium in the carbon dioxide system in seawater. *Mar. Chem.* **1999**, *65*, 135−153.
(45) Millero, F.; Huang, F.; Ggrham, T.; Pierrot, D. The dissociation of carbonic acid in NaCl solutions as a function of concentration and temperature. *Geochim. Cosmochim. Acta* **2007**, *71*, 46−55.
(46) Mills, A.; Chang, Q.; McMurray, N. Equilibrium studies on colorimetric plastic film sensors for carbon dioxide. *Anal. Chem.* **1992**, *64*, 1383−1389.
(47) Kawabata, Y. Fiber-optic sensor for carbon dioxide with a ph indicator dispersed in a poly(ethylene glycol) membrane. *Anal. Chim. Acta* **1989**, *219*, 223−229.
(48) Wolfbeis, O. S.; Kovacs, B.; Goswami, K.; Klainer, S. M. Fiber-optic fluorescence carbon dioxide sensor for environmental monitoring. *Mikrochim. Acta* **1998**, *129*, 181−188.
(49) Uttamlal, M.; Walt, D. R. A Fiber-Optic Carbon Dioxide Sensor for Fermentation Monitoring. *Bio/Technol.* **1995**, *13*, 597−601.
(50) Crank, J. *The Mathematics of Diffusion*, 2nd ed.; Oxford University Press: Bristol, 1975; p 413.
(51) Duan, Z.; Sun, R.; Zhu, C.; Chou, I. An improved model for the calculation of CO_2 solubility in aqueous solutions containing Na+, K+, Ca2+, Mg2+, Cl−, and SO42−. *Mar. Chem.* **2006**, *98*, 131−139.
(52) Cussler, E. L. *Diffusion: Mass Transfer in Fluid Systems*, 2nd ed.; Cambridge University Press: New York, 1997; p 581.
(53) Kamholz, A. E.; Schilling, E. A.; Yager, P. Optical measurement of transverse molecular diffusion in a microchannel. *Biophys. J.* **2001**, *80*, 1967−1972.
(54) Sinton, D.; Erickson, D.; Li, D. Microbubble lensing-induced photobleaching (μ-BLIP) with application to microflow visualization. *Exp. Fluids* **2003**, *35*, 178−187.
(55) Kell, G. S.; Whalley, E. Reanalysis of the density of liquid water in the range 0−150 °C and 0−1 kbar. *J. Chem. Phys.* **1975**, *62*, 3496−3503.
(56) Lao, A. I. K.; Lee, T. M. H.; Hsing, I.-M.; Ip, N. Y. Precise temperature control of microfluidic chamber for gas and liquid phase reactions. *Sens. Actuators, A* **2000**, *84*, 11−17.
(57) Guijt, R. M.; Dodge, A.; van Dedem, G. W. K.; de Rooij, N. F.; Verpoorte, E. Chemical and physical processes for integrated temperature control in microfluidic devices. *Lab Chip* **2003**, *3*, 1−4.
(58) Marre, S.; Roig, Y.; Aymonier, C. Supercritical microfluidics: Opportunities in flow-through chemistry and materials science. *J. Supercrit. Fluids* **2012**, *66*, 251−264.
(59) Luther, S. K.; Braeuer, A. High-pressure microfluidics for the investigation into multi-phase systems using the supercritical fluid extraction of emulsions (SFEE). *J. Supercrit. Fluids* **2012**, *65*, 78−86.